Crystal Structure of the High-Pressure Phase of Solid CO_2

K. Aoki,* H. Yamawaki, M. Sakashita, Y. Gotoh, K. Takemura

X-ray diffraction study of solid CO_2 at room temperature has shown that the powder pattern of the high-pressure phase, which supersedes the low-pressure cubic *Pa*3 phase at about 10 gigapascals, is consistently interpreted in terms of an orthorhombic *Cmca* structure. The orthorhombic cell at 11.8 gigapascals has dimensions of 4.330 ± 0.015, 4.657 ± 0.005, 5.963 ± 0.009 angstroms for its *a*, *b*, and *c* faces, respectively, and a volume of 120.3 ± 0.5 cubic angstroms. Four molecules contained in the unit cell are located at the base-centered positions with their molecular axes inclined at about 52° with respect to the crystallographic *c* axis. The volume change associated with the *Pa*3-*Cmca* transition is close to zero. The structural dimensions obtained for the high-pressure crystalline phase of CO_2 are of great importance for a theoretical understanding of the role of intermolecular interactions, including quadrupole-quadrupole interactions, in molecular condensation.

Carbon dioxide, CO_2, is one of the most well studied molecules. It is a symmetrical linear molecule with a very large quadrupole moment of -4.3×10^{-26} esu cm^2 (electrostatic units) (*1*). Because its molecular charge distribution is so readily characterized, CO_2 has attracted considerable attention from theorists as a prototype for understanding the role of quadrupole-quadrupole interactions in molecular condensation. For example, the crystal structure, volume compression, and vibrational property of solid CO_2 have been calculated with various model potentials and compared with experimental results to examine their validity (*2–6*). Among these predictions, a high-pressure phase transition is particularly interesting. Kuchta and Etters predicted on the basis of the cohesive energy calculation of solid CO_2 that a cubic *Pa*3 structure should transform into an orthorhombic *Cmca* structure at several gigapascals (*5, 6*). Up to date, the cubic *Pa*3 structure commonly called dry ice (*7*), which has been shown to be favored for quadrupole molecules (*2*), is the only known crystalline phase of CO_2 with a broad range of pressure and temperature.

The high-pressure behavior of solid CO_2 has been experimentally studied by optical and x-ray diffraction measurements (*8–15*). A new solid phase was first observed by Raman measurement at pressures around 18 GPa at room temperature (*12*). Subsequently, this pressure-induced transition was confirmed by Raman scattering at about 11 GPa and at temperatures below 80 K (*13*). Recent infrared absorption measurement at room temperature revealed that the phase transition occurred at about 12 GPa and that the agreement between the infrared frequencies measured for the high-pressure phase and calculated for a presumed *Cmca* structure was not satisfactory (*15*). Despite clear evidence of the high-pressure phase in the vibrational spectra, no x-ray diffraction study has succeeded in determining the crystal structure (*9–11*). Liu has observed a complicated change in the relative intensities of the diffraction peaks at about 12 GPa and pointed out the possibility of a phase transition associated with the change of the angle of tilt of the CO_2 molecules (*11*). However, a definitive conclusion concerning any change in the crystal structure was unable to be made because of the limited number of diffraction peaks observed.

We have made x-ray diffraction measurements on solid CO_2 at high pressures across the transition pressure at room temperature. High-quality powder patterns were obtained for its low- and high-pressure phases with the use of a diamond cell combined with an intense synchrotron x-ray beam and an image-plate area detector. The powder data thus obtained enabled us to determine the crystal structure of the high-pressure phase. Here, we present the details of the experimental procedure and the structure analysis. The structural aspects of the high-pressure phase are discussed in comparison with a theoretically predicted structure.

Commercially obtained gaseous CO_2 of 99.995% purity was used without further purification. The CO_2 gas was blown into the sample chamber of a gasketed diamond cell that had previously been cooled with liquid nitrogen below the sublimation temperature of 195 K. Solidified CO_2 was quickly enclosed inside the chamber and pressurized to a few gigapascals at low temperature. The diamond cell was then warmed to room temperature for observation. This loading procedure was carried out in a glove box purged with nitrogen gas in order to prevent contamination of the specimen by water and other gases.

Synchrotron x-ray diffraction measurements were performed at the Photon Factory, National Laboratory for High Energy Physics (KEK). A monochromatized beam collimated into a diameter of 40 or 80 μm was passed through the specimen, and the subsequent diffraction patterns were recorded on an image plate 200 mm by 250 mm in area. A typical exposure time was 2 hours. [Detailed description of the experimental configuration and data-processing procedure has been presented elsewhere (*16*).] All measurements were made at 295 K, and the pressure was determined by the ruby fluorescence method (*17*).

A phase transition from the cubic structure was observed at about 10 GPa. Typical diffraction patterns of the low- and high-pressure phases recorded on an image plate are shown in Fig. 1. The top pattern was taken at 7.46 GPa, and the observed reflection peaks were completely indexed on the basis of the cubic *Pa*3 structure. The derived unit cell parameter was a = 5.056 ± 0.001 Å, and the cell volume, V, was 129.3 ± 0.1 Å^3. The bottom pattern taken at 11.8 GPa differs from that of the top, which indicates that the cubic phase was transformed into the high-pressure phase. Several new reflections were observed in the low-angle region, along with a few faint reflections from the low-pressure cubic phase.

The reflection peaks from the high-pressure phase can be well interpreted in terms of an orthorhombic unit cell. The cell parameters determined from six curve-fitted peaks were a = 4.330 ± 0.015, b = 4.657

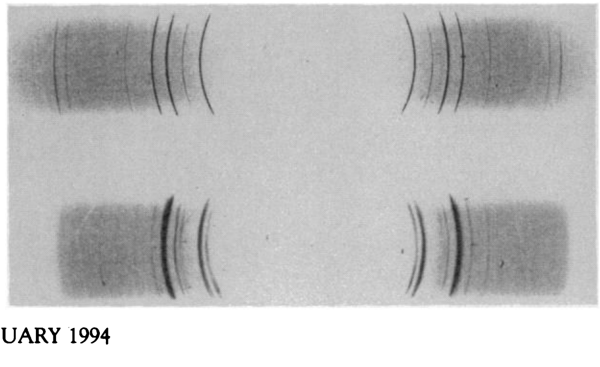

Fig. 1. X-ray powder diffraction patterns recorded on an image plate; the cubic *Pa*3 phase at 7.46 GPa is on top, and the high-pressure phase at 11.8 GPa is on the bottom.

K. Aoki, H. Yamawaki, M. Sakashita, Y. Gotoh, National Institute of Materials and Chemical Research, Tsukuba, Ibaraki 305, Japan.
K. Takemura, National Institute for Research in Inorganic Materials, Tsukuba, Ibaraki 305, Japan.

*To whom correspondence should be addressed.

± 0.005, and $c = 5.963 \pm 0.009$ Å, and the cell volume was 120.3 ± 0.5 Å^3. The number of molecules contained in the unit cell was easily derived to be four by comparison of the cell volume with the cubic *Pa*3 cell known to contain four molecules (*7*). Interplanar spacings calculated with these cell parameters are given in Table 1 together with those for the cubic structure at 7.46 GPa. At 11.8 GPa, the lattice parameter of the coexisting cubic phase was also determined to be $a = 4.939 \pm 0.010$ Å. Its cell volume, 120.5 ± 0.7 Å^3, is within the experimental accuracy nearly equal to that of the high-pressure phase.

The next step in the structural analysis was the determination of the atomic positions in the unit cell with the observed reflection intensities. For simplifying the procedure, we used a rigid molecular model in which the length of the CO_2 molecule was assumed to be fixed at 2.32 Å. In the case of the cubic *Pa*3 structure, this assumption gives a complete crystal structure and allows a straightforward intensity calculation for a given Debye-Waller factor, $\exp[-B(\sin \theta/\lambda)^2]$. Consequently, a single isotropic temperature factor *B* can be obtained by direct comparison of the observed intensities with the calculated values. A value for *B* of 6.3 Å^2 was thus determined for the cubic structure at 7.46 GPa (Table 1).

Table 1. Observed and calculated interplanar spacings and reflection intensities for the cubic *Pa*3 phase at 7.46 GPa and the orthorhombic *Cmca* phase at 11.8 GPa. The cell dimensions are $a = 5.056 \pm 0.001$ Å for the cubic structure and $a = 4.330 \pm 0.015$, $b = 4.657 \pm 0.005$, and $c = 5.963 \pm 0.009$ Å for the orthorhombic structure. An isotropic temperature factor, $B = 6.3$ Å^2, was used in the intensity calculations of both structures. Planes are indicated by *h*, *k*, and *l*; d_{obs} and d_{cal} are the observed and calculated, respectively, *d* spacing between planes; I_{obs} and I_{cal} are the observed and calculated, respectively, intensity. Dashes indicate that reliable experimental values were not obtained.

h k l	d_{obs} (Å)	I_{obs}	d_{cal} (Å)	I_{cal}
		Cubic (7.46 GPa)		
1 1 1	2.919	100.0	2.919	100.0
2 0 0	2.529	8.2	2.528	6.0
2 1 0	2.261	88.2	2.261	77.5
2 1 1	2.064	62.4	2.064	48.1
2 2 0	1.788	4.4	1.788	5.2
2 2 2	1.460	1.4	1.460	1.2
3 2 0	1.401	5.5	1.402	4.9
3 2 1	1.352	11.6	1.351	11.0
		Cubic (11.8 GPa)		
1 1 1	2.852		2.851	
2 1 0	2.212		2.209	
2 1 1	2.012		2.016	
		Orthorhombic (11.8 GPa)		
0 0 2	2.985	21	2.989	15.4
1 1 1	2.802	100	2.798	100.0
0 2 0	2.329	22	2.328	7.6
1 1 2*	2.174	105	2.172	91.2
0 2 1*			2.169	9.3
2 0 0	2.152	67	2.153	43.8
0 2 2	1.835	7	1.837	1.4
2 0 2	–	–	1.747	2.3

*These patterns overlap.

Intensity analysis for the high-pressure phase was more complicated. It seemed rather difficult to identify the most probable space group from the extinction rule of assigned reflection indices, because the number of reflections observed was only six. Instead, we chose a *Cmca* structure as a likely candidate for the high-pressure phase in accordance with theoretical prediction (*5*, *6*). The crystallization of CS_2 into a *Cmca* structure gives more support for the presumed *Cmca* structure (*18*); CS_2 is a linear molecule with a large quadrupole moment like that of CO_2 (*19*). Assuming a *Cmca* structure and a rigid molecular model greatly reduces the number of positional parameters to be determined. Finally, the atomic positions or the molecular arrangements can be defined completely with only one parameter: the angle ϕ between the molecular axis and the crystallographic *c* axis in the *bc* plane. Again, the isotropic temperature factor $B = 6.3$ Å^2 was used for the correction of the Debye-Waller factor. A good fit in reflection intensities was obtained for the *Cmca* structure with a value for ϕ of 52°, which is in exact agreement with the predicted angle (*5*).

The observed and calculated reflection intensities of the *Cmca* structure are summarized also in Table 1. The powder diffraction pattern measured at 11.8 GPa, which was obtained by integration of the intensity along each Debye-Scherrer ring recorded on an image plate, was compared with the calculated one (Fig. 2). The overall agreement between the observed and calculated profiles supports the *Cmca* structure.

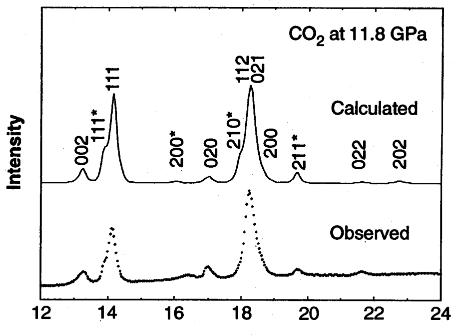

Fig. 2. Observed and calculated x-ray powder diffraction patterns of the high-pressure phase of solid CO_2. The lower pattern was taken at 11.8 GPa with an x-ray wavelength of 0.6888 Å. Reflection indices are assigned on the basis of an orthorhombic *Cmca* structure. Those with asterisks represent reflections from the coexisting cubic *Pa*3 structure.

The low- and high-pressure phases have crystal structures closely related to each other. The *Pa*3 and *Cmca* unit cells determined at 11.8 GPa are illustrated in Fig. 3. In both structures, the centers of CO_2 molecules are on the face-centered positions and a difference can be seen in their molecular orientation. The molecular axes point in the body-diagonal directions in the cubic structure, whereas they all align in the same plane parallel to the *bc* plane in the orthorhombic structure. Each structure can be converted into the other by simple transformations. The cubic structure, for instance, can be transformed into the orthorhombic structure by rotating all the molecules until they become parallel to one of the base planes and successively by deforming the unit cell from a cube to a rectangular parallelepiped.

The observed *Pa*3-*Cmca* transition provides an experimental support for the theoretically predicted sequential transition of solids composed of linear molecules with large quadrupole moments. Cohesive energy calculations on solid CO_2 have shown that the molecular arrangements appearing in the *Pa*3 and *Cmca* structures are energetically stabilized by large quadrupole-quadrupole interactions (*2*). Recent calculations have further predicted that the cubic structure, which is favored at low density,

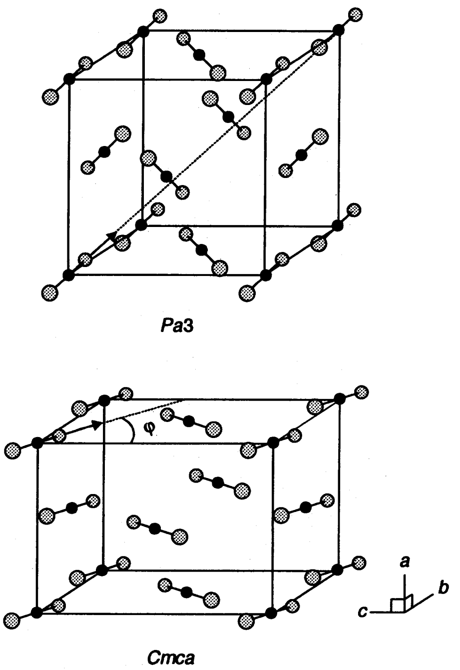

Fig. 3. The cubic *Pa*3 and orthorhombic *Cmca* structures determined at 11.8 GPa. In association with the *Pa*3-*Cmca* transition, the originally equivalent cubic *a* axis splits into the orthorhombic *a*, *b*, and *c* axes, and simultaneously the molecules tilt down on one of the base planes with their molecular axes inclined at $\phi =$ 52° from the crystallographic *c* axis.

should be transformed into the orthorhombic structure at higher density (5, 6). This is exactly what has been shown in our x-ray experiment on solid CO_2: the transition occurred at 9.9 GPa as the molar volume was densified to 18.84 $cm^3\ mol^{-1}$, about 40% denser than the volume of 26.0 $cm^3\ mol^{-1}$ at 83 K and atmospheric pressure (7). Similar pressure-induced *Pa*3-*Cmca* transitions have been found for acetylene at 0.9 GPa (*20*) and for nitrous oxide at 4.8 GPa (*21*, *22*); both are also linear molecules with large quadrupole moments comparable to that of CO_2.

The volume change on transition is shown to be very small. The molar volumes obtained for the cubic and orthorhombic phases coexisting at 11.8 GPa are 18.13 ± 0.09 and 18.10 ± 0.07 $cm^3\ mol^{-1}$, respectively. Including the uncertainty, the volume difference of 0.16 ± 0.90% is in contrast to the theoretical prediction of 2.0% (5). The calculated lattice parameters at 12 GPa and at 0 K are $a = 4.92$ Å for the *Pa*3 structure and $a = 4.17$, $b = 4.65$, and $c = 6.02$ Å for the orthorhombic structure. This calculation is in good agreement with the experiment at 11.8 GPa for the orthorhombic *b* and *c* axes. For the orthorhombic *a* axis, the agreement is far less satisfactory; the calculated value is 4% smaller than the experimental one. The comparison in lattice parameters indicates that the model potential used in the energy calculation successfully describes the interaction between the molecules closely arranged in the *bc* plane but fails for the interaction between the molecular layers stacked along the *a* axis. The discrepancy in the *a* axis may arise from insufficient description of long-range interactions, such as van der Waals forces between the molecules located in the different layers. The crystal structure determined for the high-pressure phase of solid CO_2 should be useful for refining the model potential for solid CO_2.

REFERENCES AND NOTES

1. M. R. Battaglia *et al.*, *Mol. Phys.* **43**, 1015 (1981).
2. C. A. English and J. A. Venables, *Proc. R. Soc. London Ser. A* **340**, 57 (1974).
3. K. Kobashi and T. Kihara, *J. Chem. Phys.* **72**, 3216 (1980).
4. R. LeSar and R. G. Gordon, *ibid.* **78**, 4991 (1983).
5. B. Kuchta and R. D. Etters, *Phys. Rev. B* **38**, 6265 (1988); *ibid.* **47**, 14691 (1993).
6. R. D. Etters and B. Kuchta, *J. Chem. Phys.* **90**, 4537 (1989).
7. W. H. Keesom and J. W. L. Kohler, *Physica* **1**, 167 (1934).
8. R. C. Hanson and L. H. Jones, *J. Chem. Phys.* **75**, 1102 (1981).
9. B. Olinger, *ibid.* **77**, 6255 (1982).
10. L.-g. Liu, *Nature* **303**, 508 (1983).
11. ______, *Earth Planet. Sci. Lett.* **71**, 104 (1984).
12. R. C. Hanson, *J. Phys. Chem.* **89**, 4499 (1985).
13. H. Olijnyk, H. Daufer, H.-J. Jodl, H. D. Hochheimer, *J. Chem. Phys.* **88**, 4204 (1988).
14. H. Shimizu, T. Kitagawa, S. Sasaki, *Phys. Rev. B* **47**, 11567 (1993).
15. K. Aoki, H. Yamawaki, M. Sakashita, *ibid.* **48**, 9231 (1993).
16. K. Takemura and H. Fujihisa, *ibid.* **47**, 8465 (1993).
17. H. K. Mao, P. M. Bell, J. W. Shaner, D. J. Steinberg, *J. Appl. Phys.* **49**, 3276 (1978).
18. C. W. Weir, G. J. Piermarini, S. Block, *J. Chem. Phys.* **50**, 2089 (1969).
19. Unlike the CO_2 molecule, the CS_2 molecule has a positive quadrupole moment of $+3.6 \times 10^{-26}$ esu cm^2 (*1*). It should be noted that the quadrupole-quadrupole contribution to cohesive energy is independent of the sign of moment, because the interaction between the quadrupole moments on pairs of two molecules can be shown to be proportional to the product of the moments (*2*).
20. K. Aoki *et al.*, *J. Chem. Phys.* **88**, 4565 (1988).
21. R. L. Mills, B. Olinger, D. T. Cromer, R. LeSar, *ibid.* **95**, 5392 (1991).
22. H. Olijnyk *et al.*, *ibid.* **93**, 45 (1990).
23. This work was done under proposal 93G094 of the Photon Factory, National Laboratory for High Energy Physics (KEK).

30 August 1993; accepted 1 December 1993

Wind Streaks on Venus: Clues to Atmospheric Circulation

Ronald Greeley,* Gerald Schubert, Daniel Limonadi, Kelly C. Bender, William I. Newman, Peggy E. Thomas, Catherine M. Weitz, Stephen D. Wall

Magellan images reveal surface features on Venus attributed to wind processes. Sand dunes, wind-sculpted hills, and more than 5830 wind streaks have been identified. The streaks serve as local "wind vanes," representing wind direction at the time of streak formation and allowing the first global mapping of near-surface wind patterns on Venus. Wind streaks are oriented both toward the equator and toward the west. When streaks associated with local transient events, such as impact cratering, are deleted, the westward component is mostly lost but the equatorward component remains. This pattern is consistent with a Hadley circulation of the lower atmosphere.

Earth-based observations, data from flybys, and measurements from landed spacecraft reveal that Venus has a rocky surface with an average temperature of 753 K beneath an acid-laden, predominantly CO_2 atmosphere with a surface pressure of 90 bars. Ideas about atmospheric circulation on Venus are based on cloud motions (at ≈60 km altitude) deduced from ultraviolet images taken by flyby and orbiting spacecraft (*1*–*5*), wind speeds inferred from Doppler tracking of Venera (6, 7) and Pioneer Venus (8) atmospheric probes, radio tracking of balloons (at about 50 km altitude) during the VEGA mission (9, 10), and motions of features (at about 50 km altitude) in infrared images of the planet (*11*–*13*). Zonal winds are westward with speeds of $\approx 100\ m\ s^{-1}$ at cloud heights (≈60 km altitude), decreasing approximately monotonically with proximity to the surface to speeds of $\approx 10\ m\ s^{-1}$ at a height of 10 km (*14*). No eastward winds have ever been seen in the atmosphere. Meridional winds are both northward and southward but with speeds generally not exceeding several meters per second even at cloud heights (*14*). Wind speeds at the surface are from 0.3 to 1.0 $m\ s^{-1}$ (*15*), well within the range necessary to move loose surface sand and dust (*16*).

Accordingly, the principal mode of atmospheric circulation on Venus from just above the lowest scale height (at ≈10 km altitude) to ≈100 km is a zonal retrograde (westward) superrotation of the atmosphere (*14*). However, global circulation models of the lower atmosphere (especially below ≈10 km altitude) have hitherto been mostly unconstrained because of the paucity of relevant observations. Theoretical models of the lower atmosphere circulation involve a Hadley circulation driven by solar energy deposition in the deep atmosphere, preferentially at low latitudes (*17*–*21*). This circulation involves equatorward surface winds, upflow over the equator, poleward winds aloft, and downflow at high latitudes. A similar circulation is expected in both the northern and southern hemispheres of Venus.

We report here the first observations that constrain the global circulation pattern of the lower atmosphere of Venus. These are the wind streaks seen in Magellan radar data (*22*, *23*) that result from the interaction of the atmosphere and the surface. These wind streaks not only reveal the nature of the lower atmospheric circulation but also reflect the influence of the strong westward winds of the cloud-level atmosphere.

R. Greely, K. C. Bender, P. E. Thomas, Department of Geology, Box 871404, Arizona State University, Tempe, AZ 85287–1404.
G. Schubert, D. Limonadi, W. I. Newman, Department of Earth and Space Sciences, University of California, Los Angeles, Los Angeles, CA 90024–1567.
C. M. Weitz and S. D. Wall, Jet Propulsion Laboratory, 4800 Oak Grove Drive, Pasadena, CA 91109.

*To whom correspondence should be addressed.